PHYSICAL REVIEW B **75**, 241409(R) (2007)

Gold nanostructures created by highly charged ions

J. M. Pomeroy,* A. C. Perrella,† H. Grube, and J. D. Gillaspy
National Institute of Standards and Technology, Gaithersburg, Maryland 20899, USA
(Received 14 May 2007; published 28 June 2007)

Nanometer-sized structures produced by individual highly charged ion (HCI) impacts are now reported on a high-conductivity surface, and examined by scanning tunneling microscopy (STM). Highly charged ions, e.g., Bi^{81+}, represent an exotic form of terrestrial matter with neutralization energies that can exceed 375 keV per ion, and velocities in excess of 1000 km/s from only moderate electrostatic potentials (15 kV). In the experiment presented here, a single-crystal Au(111) sample was irradiated with Xe^{25+} and Xe^{44+}, which are vastly different in their neutralization energies. They have moderate velocities (slow compared to Bohr velocity) to maximize the likelihood of observing features and similar nuclear stopping powers. STM analysis indicates that the neutralization energy is less significant in forming features on gold than reported in low-free-electron-density systems. These results support the hypothesis that gold's high free-electron density enables efficient dissipation of the HCI's potential energy.

DOI: 10.1103/PhysRevB.75.241409 PACS number(s): 68.65.−k, 61.80.Jh, 68.37.Ef, 81.40.Wx

Precisely controlled laboratory experiments with highly charged ions (HCIs) are only a couple of decades old, coinciding with an astrophysical demand for improved atomic data and an industrial need for HCI erosion rates. For astrophysics, spectroscopic studies of trapped HCIs provide benchmark data for comparison with observations of supernovae[1] and cometary or planetary x rays,[2,3] due to HCIs capturing electrons from gas and dust, respectively. On the other hand, studies of HCI-surface collisions have proven important for industrial fusion and reliability estimates of extreme ultraviolet light lithography critical components, but have also led to new approaches for lithography, by either precisely controlling HCIs,[4,5] or utilizing stochastic distributions of HCIs for the synthesis of nanodevices.[6,7]

HCI-surface collisions include the well-studied kinetic energy dissipation relevant to all atomic projectiles, but HCIs also carry many keV of neutralization (potential) energy (PE) that is delivered into only a few cubic nanometers of the surface, massively intensifying the stimulation of secondary mechanisms. Collectively, HCI-target scientific studies have identified many different mechanisms that are significantly dependent on the potential energy dissipation, e.g., secondary electron yields,[8] secondary ion yields,[9] atomic sputtering,[10] and target core-electron excitation.[11] Taken altogether, these results suggest variations in the relative strengths of different dissipation mechanisms between different materials, which we define as the energy distribution profile (EDP). (We suggest the EDP as a material specific set of prefactors for each of the different energy dissipation mechanisms, e.g., 30% PE secondary electrons, 20% PE x rays, 25% PE sputtered material, etc., for material *X*.)

The widely believed, but essentially unestablished, view is that the target material's free-electron density is the single most important parameter in determining the EDP, and, therefore, how the potential energy is dissipated. In particular, materials with low free-electron densities (long hole lifetimes) are seen to have sputter yields with strong charge state dependence,[12] and are observed to form "hillocks"[13–15] due to single ion collisions. Previous measurements of sputter yields on gold did not report a measurable increase in sputter yield,[16] and hillock formation on gold was assumed to be negligible (previous attempts by multiple groups failed). However, the scanning tunneling microscope (STM) images here (e.g., Fig. 1) represent clear evidence of nanofeatures formed by highly charged ions on gold, a free-electron material. Initially, this observation appears to challenge the assumed dependence on the free-electron density by implying strong coupling of potential energy to ionic motion, but detailed analysis presented here reveals several indicators that suggest the nuclear stopping of the ion is primarily responsible for the deformation under these conditions. This analysis of the gold nanofeatures formed by HCIs at two extremes in neutralization energy establishes (1) that the EDP for gold is different from that for insulators, and, therefore, (2) that the EDP is not constant for all materials, and, finally, (3) that free-electron density is, indeed, important in determining the EDP of a material.

In many HCI-surface studies, a common strategy is to correlate the mean object size (or sputter yield) with the potential energy per ion. In this case, the analysis of the mean object size is less meaningful due to the breadth and variety of features. Shown at the top in Fig. 2 is a STM image of the Au(111) surface after irradiation with Xe^{25+} ions, where many features are observed at a density approximately equal to the ion dose, i.e., one nanofeature per HCI impact. After

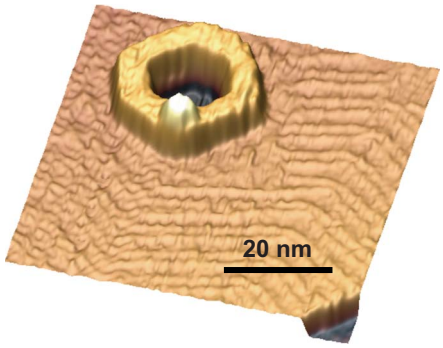

FIG. 1. (Color online) STM image of a nanofeature created by a single Xe^{44+} ion's impact on a clean Au(111) surface with 8 keV/q of kinetic energy—each distinct level is one atomic height.

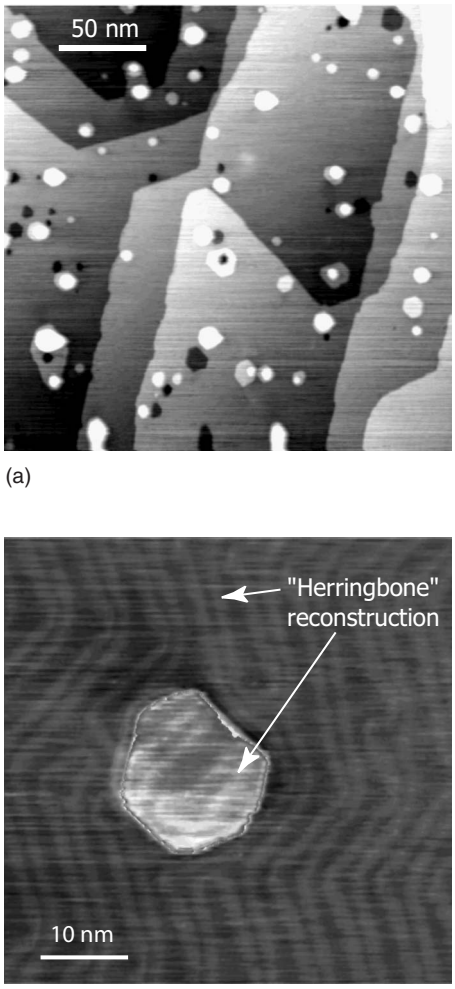

FIG. 2. Top: STM image of the Au(111) surface after exposure to Xe^{25+} ions, demonstrating a diversity of nanofeatures (contrast levels are one atomic height). Bottom: STM image of a single feature showing the $22\times\sqrt{3}$ reconstruction around and *on top* of the hexagon formed by the impact of a single Xe^{25+} ion; the island is one atomic layer high (a discontinuous color map is used to emphasize the reconstruction on the two atomic levels).

an ion collides, the impact zone thermally equilibrates in a few picoseconds,[17] i.e., it forms hexagons. One can easily find at least three different classes of unique object types, e.g., isolated hexagons, hexagonal rings with craters in the center, and hexagonal islands with pits (atomic vacancy clusters) immediately adjacent. The hexagonal shapes form during the relaxation after the ion's impact to align with the crystal's low-index directions. For comparison of the object size distributions, all feature types are considered equally, and the average displaced volume per feature is calculated; data for Xe^{25+} and Xe^{44+} extracted at 8 kV are shown in Table I. These two conditions are a factor of 6.5 different in potential energy, but differ by only 3% in nuclear stopping power[25] (a factor of 1.5 difference in kinetic energy that goes into electronic stopping power). The mean object sizes scale similar to nuclear stopping powers. The weak dependence on kinetic energy (due to the peak in nuclear stopping power) is

TABLE I. Mean feature size and standard deviation for nanofeatures formed by Xe^{25+} and Xe^{44+} extracted at 8 kV along with the corresponding kinetic (KE) and potential (PE) energies per ion and the nuclear stopping power.

HCI	PE (keV)	KE (keV)	Nuclear stopping (keV/nm)	Mean size (nm^3)	Standard deviation (nm^3)
Xe^{25+}	8	200	5.7	23.6	17.2
Xe^{44+}	51	350	5.9	26.9	18.9

also consistent with kinetic energy data from Parks *et al.*,[18] while, in contrast, no saturation in the potential energy scaling for insulators has been observed in this energy range.[14] Surface images from the molecular dynamics simulations by Bringa *et al.*[19] and other experimental data of singly charged xenon in the same kinetic energy range find features of a size and structure very similar[20] to (although slightly smaller than) those reported here. The "mean crater area" in that work at 400 keV of kinetic energy with no potential energy is listed as 34 nm^2, and the crater size in Fig. 1 is ≈40 nm^2. Since the (111) face used in this work does not provide open crystal channels, it is expected that more collisions will occur close to the surface [compared to the (100) face in the simulation], and result in a somewhat larger average size for surface features. In addition, the distribution of feature sizes and types suggests that the ion's impact parameter with respect to the atomic lattice is important, whereas potential energies of this magnitude result in classical electron flow at nanometers from the surface, effectively washing out microscopic variations.[21]

Another more subtle piece of evidence is shown in the lower frame of Fig. 2, where the $22\times\sqrt{3}$ "herringbone" reconstruction is observed both around and on top of a hexagon formed by the impact of a single Xe^{44+} ion, which implies that the island's atoms came from deep in the bulk. The herringbone reconstruction spontaneously forms on the atomically flat Au(111) face to relax compressive stresses by allowing atoms to occupy both hcp and fcc lattice positions.[22] The reconstruction is easily disrupted by atomic vacancies,[23] since the vacancies change the compressive strain field. The island shown is composed of more than 3000 surface atoms, and the same number of corresponding vacancies must be present somewhere in the crystal (by conservation of mass), yet the local vacancy density is apparently low enough that the reconstruction is not disrupted. Since the potential energy during neutralization transfers into only a few cubic nanometers of the surface around the impact site, the absence of these defects would require the long-range migration of 3000 vacancies with little adatom annihilation, a very low-probability event. On the other hand, defects produced by kinetic energy stopping will be distributed along the ion channel, and interstitial atoms can migrate preferentially along the track to the surface, while the corresponding vacancies can either annihilate at surface steps or form metastable clusters in the bulk.[24]

Further evidence that the vacancies are being produced deep within the lattice (due to the kinetic energy) rather than

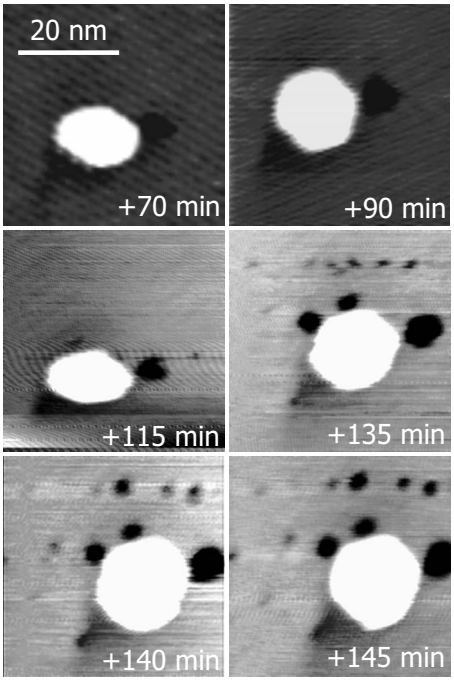

FIG. 3. STM images of the same nanofeature at various times after ion irradiation. While the feature is initially observed with only one adjacent pit, additional pits form and grow in later images—the island is three atomic layers high, and some pits are multiple layers deep.

on the surface is shown in the sequence of STM images in Fig. 3. The central feature is a large island that is three atomic layers high (the color scale is adjusted in most of the images to emphasize the changes in the surrounding terrace). In the first two images, only one pit a single atomic layer deep is observed to the upper right of the island, although some other lattice deformation is evident.[26] Between the second and the fourth images, several additional pits appear, and some have coalesced. In the final two images, the existing pits grow in breadth and depth, but otherwise remain essentially stable. This sequence captures atomic vacancies "bubbling" up from deep in the lattice.

This evidence indicates the features formed primarily due to the nuclear stopping of the HCI. The feature size data presented in Table I are correlated with the nuclear stopping component (little change), but are uncorrelated with the potential energy, even though it changes by more than a factor of 6. Further, the similarity in size and structure to features observed in molecular dynamics simulations and experimental data of singly charged xenon in this kinetic energy range supports this conclusion. The broad distributions of feature sizes and types imply that the details of the ion's impact parameter with the surface's atomic lattice are important, further implicating kinetic energy as dominant. Finally, precise analysis of the nanofeatures provides indications that the atoms observed that compose the nano-structures originated from deep within the crystal: the reconstruction observed on some islands and the percolation of defects to the surface over the course of hours both support this hypothesis. Taken all together, we conclude that, in this energy regime, mechanisms deriving from kinetic energy dissipation dominate the surface deformation, while little dependence is seen on potential energy.

This conclusion, while consistent with previously reported sputter data[16] on gold, does not eliminate the the possibility that potential energy could play a role in surface deformation of free-electron metals, but does show that it is almost certainly much weaker than the nuclear stopping effect. This result stands in stark contrast to results for insulating materials and even graphite, where potential energy deformation was found to be much stronger than kinetic energy mechanisms. Therefore, the EDP for gold is clearly different from that for those materials.

Broadly speaking, this starkly different EDP provides strong evidence that the target free-electron density is important. By comparison to insulators, the relatively high density of free electrons in metals, only a few eV below the vacuum energy, translates to fast electron transfer occurring while the ion is farther from the surface. This provides the surface with more time to relax with less depletion of the electron density at those shallow levels (near the Fermi energy). Earlier electron transfer also provides the HCI with more time to reduce its energy by secondary electron shedding and relaxation to the core, via x rays or ultraviolet radiation. The potential energy remaining when the ion reaches the surface can also be more easily absorbed by the fast response of the metal's electron sea. Conversely, the depletion of shallow electron levels in semimetals and insulating materials results in more potential energy transferred to the lattice, i.e., more lattice deformation and more internal stress.

With this analysis, we have presented evidence that irradiation of a gold surface by HCIs can produce nanofeatures similar to those previously reported on surfaces with low free-electron densities. Careful analysis of these features reveals that the primary formation mechanisms are likely driven by the HCI's kinetic energy (nuclear stopping), not its potential energy, demonstrating that the free-electron density is an important parameter in determining any material's response to HCI neutralization. When this result is considered along with other published HCI-surface data, it is clear that different materials must have different EDPs, i.e., dissipate the eletronic energy more efficiently through mechanisms that depend on the target material. So, whether one's interest in HCI-matter interactions derives from observations of cosmological events, basic atomic physics, or the desire to manufacture nanofeatures, accurate quantitative interpretation of data requires deconvolving the EDP from the result.

*joshua.pomeroy@nist.gov
†Deceased.

[1] U. Hwang *et al.*, Astrophys. J. Lett. **516**, L117 (2004).
[2] T. E. Cravens, Science **296**, 1042 (2002).
[3] I. P. Robertson and T. E. Cravens, J. Geophys. Res. **108**, LIS6 (2003).
[4] N. Stolterfoht, J. H. Bremer, V. Hoffmann, R. Hellhammer, D. Fink, A. Petrov, and B. Sulik, Phys. Rev. Lett. **88**, 133201 (2002).
[5] A. Persaud, S. J. Park, J. A. Liddle, T. Schenkel, J. Bokor, and I. W. Rangelow, Nano Lett. **5**, 1087 (2005).
[6] J. M. Pomeroy, H. Grube, A. C. Perrella, and J. D. Gillaspy, Nucl. Instrum. Methods Phys. Res. B **258**, 189 (2007).
[7] T. Schenkel, A. Persaud, S. J. Park, J. Nilsson, J. Bokor, J. A. Liddle, R. Keller, D. H. Schneider, D. W. Cheng, and D. E. Humphries, J. Appl. Phys. **94**, 7017 (2003).
[8] D. G. H. Schneider and M. A. Briere, Phys. Scr. **53**, 228 (1995).
[9] T. Schenkel, A. V. Barnes, M. A. Briere, A. Hamza, A. Schach von Wittenau, and D. H. Schneider, Nucl. Instrum. Methods Phys. Res. B **125**, 153 (1997).
[10] T. Schenkel, A. V. Hamza, A. V. Barnes, and D. H. Schneider, Prog. Surf. Sci. **61**, 23 (1999).
[11] J. P. Briand, S. Thuriez, G. Giardino, G. Borsoni, M. Froment, M. Eddrief, and C. Sebenne, Phys. Rev. Lett. **79**, 2591 (1997).
[12] G. Hayderer *et al.*, Phys. Rev. Lett. **86**, 3530 (2001).
[13] C. Ruehlicke, M. A. Briere, and D. Schneider, Nucl. Instrum. Methods Phys. Res. B **99**, 528 (1995).
[14] D. C. Parks, M. P. Stockli, E. W. Bell, L. P. Ratliff, R. W. Schmieder, F. G. Serpa, and J. D. Gillaspy, Nucl. Instrum. Methods Phys. Res. B **134**, 46 (1998).
[15] I. C. Gebeshuber, S. Cernusca, F. Aumayr, and H. P. Winter, Nucl. Instrum. Methods Phys. Res. B **205**, 751 (2003).
[16] G. Hayderer, S. Cernusca, V. Hoffmann, D. Niemann, N. Stolterfoht, M. Schmid, P. Varga, H. P. Winter, and F. Aumayr, Nucl. Instrum. Methods Phys. Res. B **182**, 143 (2001).
[17] J. M. Pomeroy, J. Jacobsen, C. C. Hill, B. H. Cooper, and J. P. Sethna, Phys. Rev. B **66**, 235412 (2002).
[18] D. C. Parks, R. Bastasz, R. W. Schmieder, and M. Stockli, J. Vac. Sci. Technol. B **13**, 941 (1995).
[19] E. M. Bringa, K. Nordlund, and J. Keinonen, Phys. Rev. B **64**, 235426 (2001).
[20] S. E. Donnelly and R. C. Birtcher, Phys. Rev. B **56**, 13599 (1997).
[21] J. Burgdorfer, P. Lerner, and F. W. Meyer, Phys. Rev. A **44**, 5674 (1991).
[22] C. Wöll, S. Chiang, R. J. Wilson, and P. H. Lippel, Phys. Rev. B **39**, 7988 (1989).
[23] A. J. Couture, Ph.D. thesis, Cornell University, 2000.
[24] P. Ehrhart, in *Numerical Data and Functional Relationships in Science and Technology*, edited by H. Ullmaier, Landolt-Börnstein, New Series, Group III: Crystal and Solid State Physics, Vol. 25 (Springer-Verlag, Berlin, 1991), pp. 88–397.
[25] Stopping powers calculated with SRIM2006 [J. F. Ziegler and J. P. Biersack, computer code SRIM2006 (United States Naval Academy, Annapolis, MD, 2006)], http://www.srim.org
[26] Images were collected at 0.2 V bias with 2 nA tunnel current. The first image was taken as part of a survey at much lower resolution. The vertical compression and diagonal lines in the third image are due to a turbo pump decelerating during image acquisition.